

Northumbria Research Link

Citation: Shalvey, T. P., Shiel, H., Hutter, Oliver, Zoppi, Guillaume, Bowen, L., Dhanak, V. R. and Major, J. D. (2022) Sodium Fluoride Doping Approach to CdTe Solar Cells. ACS Applied Energy Materials, 5 (4). pp. 3888-3897. ISSN 2574-0962

Published by: American Chemical Society

URL: <https://doi.org/10.1021/acsaem.1c03351>
<<https://doi.org/10.1021/acsaem.1c03351>>

This version was downloaded from Northumbria Research Link:
<https://nrl.northumbria.ac.uk/id/eprint/48119/>

Northumbria University has developed Northumbria Research Link (NRL) to enable users to access the University's research output. Copyright © and moral rights for items on NRL are retained by the individual author(s) and/or other copyright owners. Single copies of full items can be reproduced, displayed or performed, and given to third parties in any format or medium for personal research or study, educational, or not-for-profit purposes without prior permission or charge, provided the authors, title and full bibliographic details are given, as well as a hyperlink and/or URL to the original metadata page. The content must not be changed in any way. Full items must not be sold commercially in any format or medium without formal permission of the copyright holder. The full policy is available online: <http://nrl.northumbria.ac.uk/policies.html>

This document may differ from the final, published version of the research and has been made available online in accordance with publisher policies. To read and/or cite from the published version of the research, please visit the publisher's website (a subscription may be required.)

A Sodium Fluoride Doping Approach to CdTe Solar Cells

T. P. Shalvey^a, H. Shiel^a, O. S. Hutter^b, G. Zoppi^b, L. Bowen^c, V. R. Dhanak^a, J. D. Major^{*a}

^aStephenson Institute for Renewable Energy, Physics Department, University of Liverpool, Liverpool, L69 7ZF, UK

^bDepartment of Mathematics, Physics and Electrical Engineering, Ellison Building, Northumbria University, Newcastle Upon Tyne, NE1 8ST, UK

^cDepartment of Physics, Durham University, South Road, Durham, DH1 3LE, UK

Abstract

Sodium is a common impurity in CdTe solar cells, yet there are relatively few reports investigating its effect on complete device structures. There is the potential for uncontrolled sodium incorporation, either from impurities in the CdTe material itself or contaminants introduced during device processing, which can affect the optoelectronic properties of CdTe. Therefore, it is important to consider the impact of sodium incorporation on device performance. In this work, we show that the deposition of a thin layer of NaF at the back surface of CdS/CdTe devices prior to metallisation is an effective strategy to form a highly doped back surface and improve contact quality. High temperature ($\sim 300^\circ\text{C}$) annealing is required to effectively incorporate sodium throughout the device and improve the bulk doping density, however this also leads to sodium accumulation in the CdS layer and the formation of a TeO_2 layer at the back surface. We also find evidence of out-diffusion of sodium from commonly used TEC glass substrates at typical CdTe processing temperatures, despite the presence of an alkali diffusion barrier layer. Understanding this prevalent sodium diffusion in this class of solar cells is vital for further improvement of CdTe structures.

Keywords: CdTe, Solar Cells, Sodium, Doping, NaF

1. Introduction

Cadmium telluride (CdTe) solar cells have reached a record efficiency of 22.1%, with recent gains mainly resulting from increases in short circuit current density (J_{sc}) [1]. The open circuit voltage (V_{oc}) of record devices remains around ~ 850 mV, with little improvement in the past 20 years. These record devices have historically relied on depositing a thin (~ 1 nm) layer of copper at the back surface prior to metallization [2, 3] to both dope the bulk CdTe layer and form a p^+ region at the back surface to facilitate a quasi-ohmic contact. To further improve efficiencies, there has been a shift of research focus away from using copper doping due to strong self-compensation effects which limit hole densities to around 10^{15} cm^{-3} , and fast diffusivity which causes long term stability concerns [3, 4]. Much of this research has focused on Cd rich growth and doping on the Te site using Group V elements. Phosphorous and arsenic have been effective in achieving high doping densities ($>10^{16}$ cm^{-3}) with long carrier lifetimes in single crystal CdTe due to high activation ratios despite self compensation by AX centres [5, 6], and more recent efforts have achieved similar doping densities in polycrystalline devices [7, 8].

Whilst Group V doping has shown promise, there has been comparatively few reports of the effects of Group IA alkali metals on CdTe device performance. An understanding of the effect of sodium is especially relevant from a CdTe module manufacturing perspective, since soda lime glass substrates are typically used to lower

16 production costs. These substrates contain around 16% Na₂O [9] which can diffuse through to subsequently
17 deposited adjacent layers. Although alkali barriers such as SiO₂ are typically used to prevent this [10], they are not
18 fully effective and diffusion of sodium has been measured despite their presence, especially at high temperatures
19 such as those seen during typical CdTe deposition processes [11]. Therefore, it is vital to understand the effect
20 sodium has on device performance.

21 Substitution of Na onto Cd sites results in *p*-type doping with an acceptor level 59 meV above the valence
22 band, which is more favourable for achieving high doping densities compared to 160 meV in the case for copper
23 [12]. Although interstitial incorporation of sodium would cause compensation and potentially limit the ability to
24 dope highly *p*-type, this donor level is similarly close to the conduction band, and is therefore not likely to be a
25 lifetime limiting defect [12]. The doping efficacy of sodium has been demonstrated in single crystal CdTe devices,
26 where a doping density of $7 \times 10^{15} \text{ cm}^{-3}$ enabled a V_{oc} of 929 mV [13]. However, incorporating sodium into
27 polycrystalline films has had mixed success, with efforts focused on combining the chloride treatment and doping
28 process. Whilst an increased doping density was measured to $\sim 10^{15} \text{ cm}^{-3}$ upon sodium inclusion, this also has
29 deleterious effects on film morphology. This includes agglomeration of CdS window layer leading to a poor diode
30 response, and widening of CdTe grain boundaries thereby shorting contacts, which has so far limited study at a
31 device level [14–18].

32 Here we report on the incorporation of sodium into CdS/CdTe devices by thermally evaporating a thin layer
33 of NaF prior to contacting. By depositing NaF after the chloride treatment, the excessive recrystallisation which
34 has been problematic in previously reported attempts is avoided [14–18]. In this work, this has improved the
35 back contact as shown by the absence of 'rollover' in current density - voltage (JV) curves, implying a more
36 highly doped region localised at the back surface. Annealing these devices in air at temperatures greater than
37 300°C causes sodium to diffuse into the bulk CdTe region, whereby a small increase in acceptor concentration is
38 measured.

39 2. Experimental Methods

40 Devices were fabricated on TEC 15M commercial soda-lime glass substrates which are coated by the manu-
41 facturer with an alkali blocking layer, as well as SnO₂:F (FTO) which acts as a transparent front contact, and a
42 nominally undoped SnO₂ buffer layer. After cleaning, 100 nm CdS was deposited via sputtering at a power density
43 of 0.32 W cm^{-2} in 5 mTorr of Ar at a substrate temperature of 200°C. CdTe was then deposited by close spaced
44 sublimation (CSS), with a source and substrate temperature of 610°C and 510°C respectively. This is performed in
45 a two step process, with the main deposition occurring under 30 Torr nitrogen yielding a thickness of 4 - 5 μm after
46 25 min, followed by a short 30 s deposition under vacuum in order to encourage nucleation and fill any pinholes.
47 Samples were etched in a dilute nitric-phosphoric acid (NP etch) for 30 s prior to MgCl₂ treatment at 410°C in
48 air [19]. A second NP etch was then performed for 15 s before rinsing in deionised water. For samples which
49 included an NaF layer, this was deposited by thermal evaporation, with thickness monitored by a quartz crystal
50 microbalance. Copper was intentionally omitted from the device structure to minimise the number of variables
51 under study and hence we anticipate a lower overall cell performance, yet this allows for a clearer comparison of
52 devices. Devices which were subject to annealing were placed onto a pre-heated hotplate in air for 20min before

53 being removed and allowed to cool to room temperature. A 50 nm Au back contact was then thermally evaporated
54 through a mask to define nine 0.25 cm² contacts per device. Front contacts are made by mechanically scraping
55 the CdTe layer, and removing CdS with HCl to expose the underlying FTO front contact.

56 Test structures to examine out-diffusion of sodium from soda-lime glass substrates were fabricated by deposit-
57 ing CdTe directly onto cleaned TEC 15M substrates. The growth rate was controlled by varying the nitrogen
58 pressure in the CSS chamber between 5 - 400 Torr, with higher pressures acting to reduce the Cd and Te partial
59 pressures and therefore slow the growth rate [20]. This resulted in growth times between 4 - 262 min to deposit a
60 7 μm CdTe layer, during which time the substrate temperature was maintained at 550°C.

61 JV measurements taken with a Keithley 2400 source meter and TS Space Systems solar simulator (class
62 AAA) calibrated to AM1.5G spectrum at 1000 W m⁻¹. EQE measurements were taken using a Bentham PVE300
63 characterisation system. Capacitance - voltage (CV) measurements were taken in the dark using a Solartron
64 SI1260 impedance analyser with an AC perturbation amplitude of 30 mV and frequency of 100 kHz, and varying
65 DC bias between -0.5 to +0.5 V. Secondary ion mass spectroscopy (SIMS) was used to obtain elemental depth
66 profiles. An ION-TOF ToF-SIMS V instrument was used for time of flight SIMS measurements of NaF treated
67 CdTe devices, and compared to ion implanted reference samples to quantify elemental concentrations of sodium,
68 fluorine and chlorine. The depth profiling beam was 1 keV Cs⁺ operated with a raster size of 200 μm². Qualitative
69 SIMS measurements of sodium diffusion from TEC glass substrates into CdTe films were performed using a Hiden
70 Analytical gas ion gun and quadrupole detector. A beam of O²⁻ ions rastered over a 500 × 500 μm² area (with an
71 11% gating to reject side wall effects) was used to sputter the sample using a beam energy of 5 keV at a current of
72 300 nA.

73 SEM images showing the back surface of sample were obtained using a JEOL7001F electron microscope,
74 whilst cross-sections were prepared via focused ion beam milling using a FEI Helios Nano Lab 600 Dual Beam
75 system, equipped with a focused 30 keV Ga liquid metal ion source. XPS was used to investigate the surface chem-
76 ical composition using an Al Kα x-ray source (hν = 1486.6 eV) operating at 200 W and a hemispherical Scienta
77 SES200 electron energy analyser comprised of a double channel plate and phosphor screen with a CCD camera.
78 The resolution was determined to be 0.7 eV, allowing binding energy determination with a precision of ±0.1 eV,
79 by fitting the Fermi edge of a reference Ag sample. Core level spectra were fitted with a Gaussian/Lorentzian
80 product function to approximate a Voigt function after removal of a Shirley background.

81 **3. Results and Discussion**

82 *3.1. NaF post deposition treatment*

83 A series of 8 CdS/CdTe devices were initially fabricated in an identical manner to each other. Following
84 MgCl₂ treatment and NP etching, 1 nm NaF was evaporated onto the back surface of 7 of these devices, and either
85 left unannealed, or annealed on a hotplate for 20 mins in air at temperatures between 100°C and 350°C before
86 contacting with Au. The remaining device was left without any NaF layer or anneal to serve as a reference for
87 comparison. The 1nm NaF thickness was chosen based on preliminary experiments (Figures S1 and S2). This
88 contacting process, whereby a few nm of a *p*-type dopant is evaporated onto the back surface prior to annealing in
89 air, matches closely to that of typical copper-contacted CdTe solar cells [21][22].

90 Figure 1 shows JV curves from the highest efficiency cell of each of these devices subject to different anneal
 91 conditions compared to a control device without NaF. There is little difference between the shape of curves corre-
 92 sponding to the NaF treated devices, although the device annealed at 350°C shows noticeably poorer performance.
 93 Since it is difficult to observe trends directly from these JV curves, a more detailed discussion of the effect of an-
 94 neal temperature on device performance is deferred to Figure 2. However, there are some obvious differences in
 95 the shape of JV curves with and without NaF treatment, irrespective of the annealing temperature. Most notably,
 96 there is a striking difference between the shape of the curves in forward bias. The control device shows rollover
 97 above V_{oc} , which is characteristic of a secondary barrier at the back contact, and is typical for a simple CdTe/Au
 98 contact structure [23]. In contrast, all devices with NaF applied at the back contact do not show such behaviour re-
 99 gardless of whether they are annealed or not, which suggests these devices have a reduced Schottky barrier. There
 100 is also a lower series resistance for NaF treated devices which can be observed from a steeper gradient around V_{oc}
 101 leading to an improved fill factor which is consistent with a lower contact barrier.

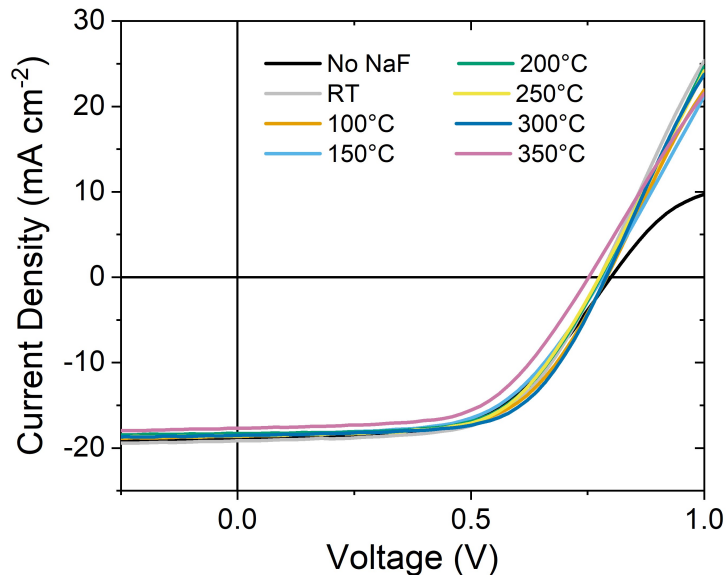


Figure 1: JV curves for the highest efficiency cell from devices with 1 nm NaF deposited prior to contacting and either left unannealed (RT), or annealed in air for 20 min at temperatures up to 350°C, compared to a device without NaF

102 This improvement in contacting is attributed to a highly doped back surface which results in a narrower barrier
 103 through which carriers can tunnel through to be extracted. In this case, it is unsurprising that the doping of the
 104 back contact is less dependent on anneal temperature since it is not necessary to redistribute the sodium into the
 105 bulk of the device at an elevated temperature, whilst the Te rich region formed at the back surface during etching
 106 means there are plenty of available Cd site to form Na_{Cd} acceptors. A similar strategy is commonly employed
 107 for copper doping in CdTe, whereby the back contact region is highly doped to form a p^+ region to assist the
 108 formation of an ohmic contact [2]. Replacing copper at the back contact with a different p -type dopant such as
 109 sodium is highly desirable, since copper can also incorporate on interstitial sites and form deep level defects in
 110 CdTe which are detrimental to device performance, and also cause long-term stability issues [4, 24]. On the other
 111 hand, DFT calculations suggest the interstitial sodium defect level is much shallower, albeit similarly acting as a
 112 donor [12]. Therefore, whilst Na_i defects are ideally avoided entirely since they compensate p -type doping, they

113 are not expected to act as strong recombination centres and so will be less harmful. The reduced rollover shown
114 in Figure 1 following NaF treatment is therefore encouraging as this shows potential as a copper-free contact to
115 CdTe. There are indications from literature reports that the presence of sodium in a CdTe device structure may
116 pose long-term stability issues [13, 25], although preliminary tests show no accelerated degradation relative to
117 NaF-free reference devices (Figure S3).

118 Figure 2 shows the average performance parameters as well as those of the highest efficiency cell for devices
119 with 1 nm NaF as a function of annealing temperature compared to a control device without NaF. For all devices
120 with NaF there is a decrease in both the average and peak V_{oc} and J_{sc} with increasing annealing temperature.
121 However, there does appear to be a small reversal of this trend around 300 °C that is especially visible in the
122 highest efficiency cell series. In contrast, the fill factor tends to be increased for those devices containing NaF.
123 This can mainly be attributed to a reduction in the series resistance of devices with NaF compared to the control
124 device. This is most apparent for the un-annealed device but is evident for all NaF treatments, since the series
125 resistance of the best cell remains lower in all cases than the control device, albeit with more variation with higher
126 anneal temperatures. The shunt resistance appears to initially increase before peaking before around 200°C, and
127 although increased shunt resistance will lead to a higher fill factor, the increase in this device series is dominated
128 by the lower series resistance. The combined effect of all these parameter changes with temperature means there
129 is little overall change in the efficiency. Some of the higher temperature anneal devices suffered from several
130 ‘shunted’ cells, which lowers the average efficiency, however in general the peak efficiency of cells tends to be
131 slightly increased for most anneal temperatures, especially at 300°C.

132 Despite the large spread of values common for laboratory made solar cells with various processing steps, it is
133 clear that the addition of NaF is not causing a drastic reduction in device efficiency as seen previously [14, 18],
134 whilst improving the quality of the back contact. This suggests that the excessive recrystallisation which proved
135 detrimental to device performance in previous attempts at sodium incorporation in CdTe devices is avoided by
136 depositing NaF after the chlorine treatment. This is supported by x-ray diffraction measurements (Figure S4) and
137 electron microscopy (Figure S5) of films with thicker (5 nm) NaF layers, which is expected to exaggerate the
138 influence of NaF incorporation, yet show no indication of significant structural changes.

139 Figure 3 shows external quantum efficiency (EQE) data for the highest efficiency cells from the NaF treated
140 devices described previously. The EQE curves shown in Figure 3a are normalised to maximum collection effi-
141 ciency for ease of comparison in Figure 3b, and show very little difference in the CdS shoulder region at short
142 wavelength. In previous attempts which have incorporated sodium into CdS/CdTe devices prior to the chlorine
143 treatment, there has been significant recrystallization at the interface [14, 15, 18], consuming the CdS layer which
144 manifests itself as an increase of EQE in the short wavelength region. Since there is no such effect observed here,
145 it is likely that the CdS layer remains intact and therefore can create a suitable junction with CdTe which can
146 effectively separate charge carriers.

147 The long wavelength region of the normalised EQE curves shows a subtle trend with anneal temperature. This
148 can be seen more easily in Figure 3c which focuses on the shoulder region whereby collection efficiency decreases
149 as the photon energy decreases below that of the CdTe band gap. To show the effect of NaF treatment on this long
150 wavelength region more clearly, Figure 3d plots the gradient along the top of the normalised EQE curves between

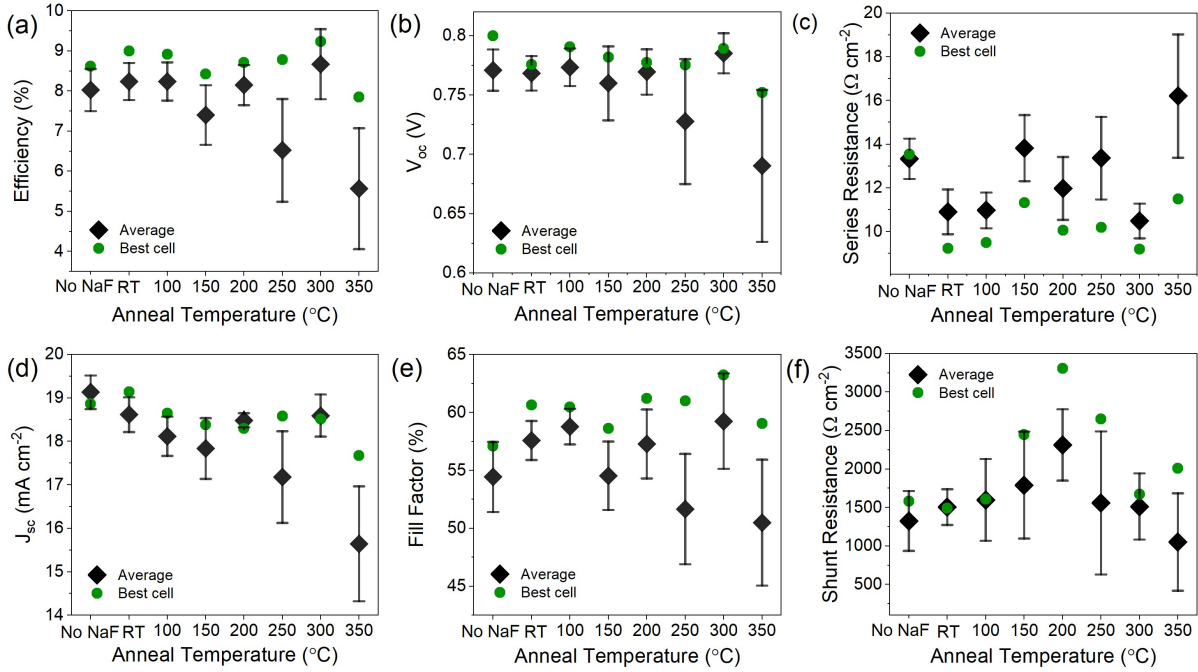


Figure 2: JV parameters showing (a) efficiency, (b) open circuit voltage (V_{oc}), (c) series resistance, (d) short circuit current density (J_{sc}), (e) fill factor and (f) shunt resistance of devices with 1 nm NaF evaporated prior to contacting and annealed for 20 min at various temperatures. Average values are shown with error bars corresponding to the standard deviation from nine 0.25 cm^2 cells per device, as well as the parameters for the highest efficiency cell from each device.

151 650-800 nm, and the gradient corresponding to the CdTe bandgap cut-off between 825-850 nm, as a function of
 152 NaF anneal temperature. Together these values give an indication of the ‘squareness’ of the EQE response at long
 153 wavelengths which corresponds to how well carriers are separated from deeper in the CdTe layer. With increasing
 154 anneal temperature, the top of the EQE curves become flatter (i.e. 650-800 nm gradient is less negative), whilst
 155 the CdTe bandgap cut-off becomes steeper (825-850 nm gradient is more negative). This means there is more
 156 efficient collection at long wavelength with increasing anneal temperature up to 250°C , where the trend is then
 157 reversed. This could result from a number of changes in the device, but given the results from capacitance-voltage
 158 measurements shown later in Figure 4, this is likely caused by a changes in depletion width allowing more efficient
 159 collection further into the CdTe layer.

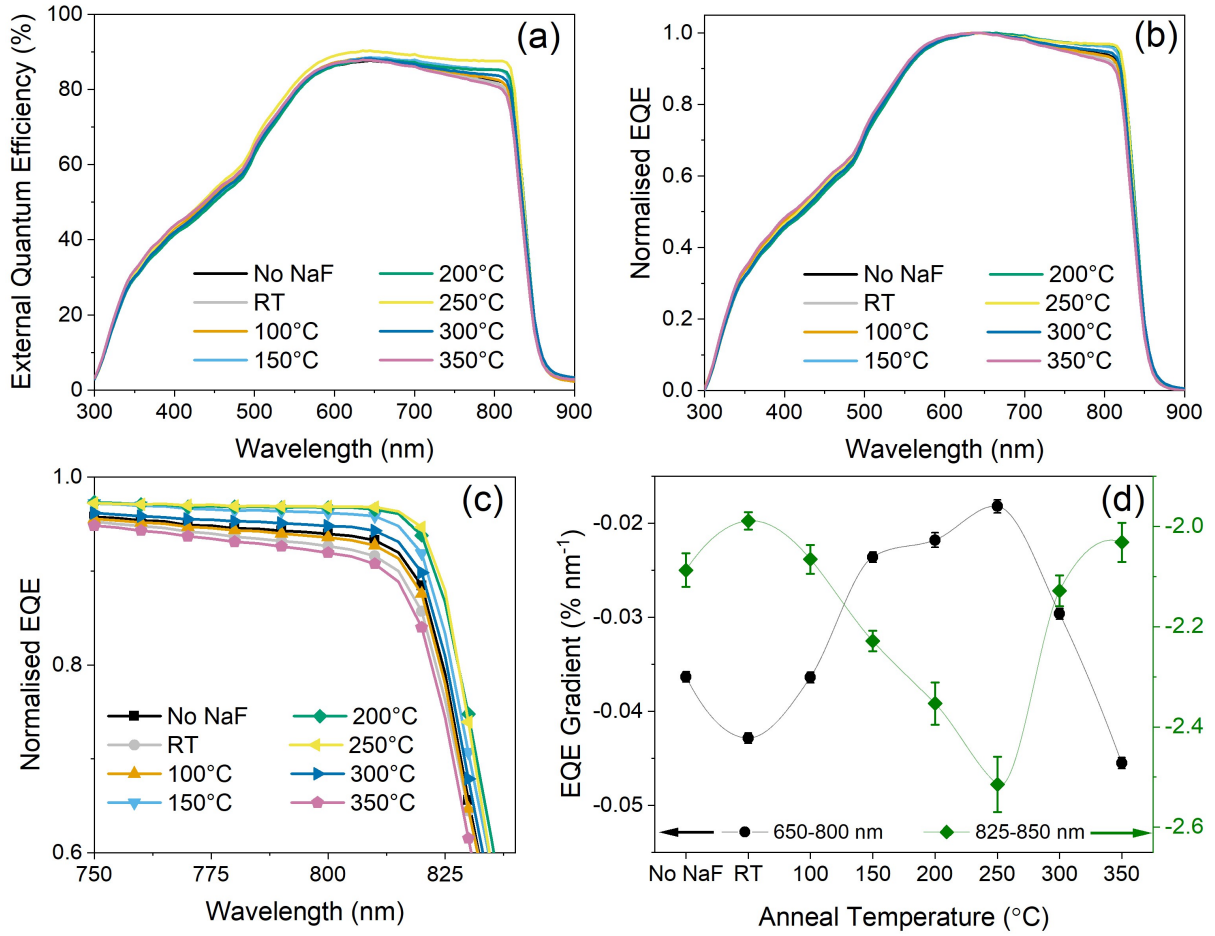


Figure 3: (a) Raw and (b) normalised EQE curves for champion cells from devices with 1 nm NaF deposited prior to contacting and annealed up to 350°C, compared to a control device without NaF. (c) shows the long wavelength region between 750-840 nm in more detail. (d) shows the gradient of the curves at long wavelength corresponding to the flat top and bandgap cut-off, representing the 'squareness' in this region with lines connecting datapoints shown as a guide to the eye.

160 Capacitance-voltage measurements were performed on the best performing cell on each device, from which
 161 the doping density as a function of depletion width can be determined as shown in Figure 4a. There is a change in
 162 both doping density and depletion width with annealing temperature, which can be seen clearer in Figure 4b. With
 163 the addition of NaF at the back surface and subsequently annealing at temperatures up to 250°C there is a decrease
 164 in the bulk acceptor concentration, which implies that rather than forming acceptor levels by occupying Cd sites,
 165 it is instead forming compensating defects that act to reduce the overall doping density, likely by incorporating
 166 interstitially into the CdTe lattice. Above 250°C there is a sharp reversal of this trend with the acceptor con-
 167 centration increasing with anneal temperature, reaching a maximum of a 50% increase compared to the control
 168 device without NaF. At this temperature, it appears the incorporation onto Na_{Cd} sites is energetically favourable
 169 compared to Na_i incorporation, thereby increasing the doping density. Since the maximum temperature used in
 170 this study was limited to 350°C it remains unclear whether higher temperatures would facilitate higher doping
 171 densities, however preliminary test devices showed reduced performance due to the presence of a heavily oxidised
 172 back surface that accompanies the higher anneal temperatures.

173 The depletion width varies inversely with acceptor concentration, since lower doping density requires a larger

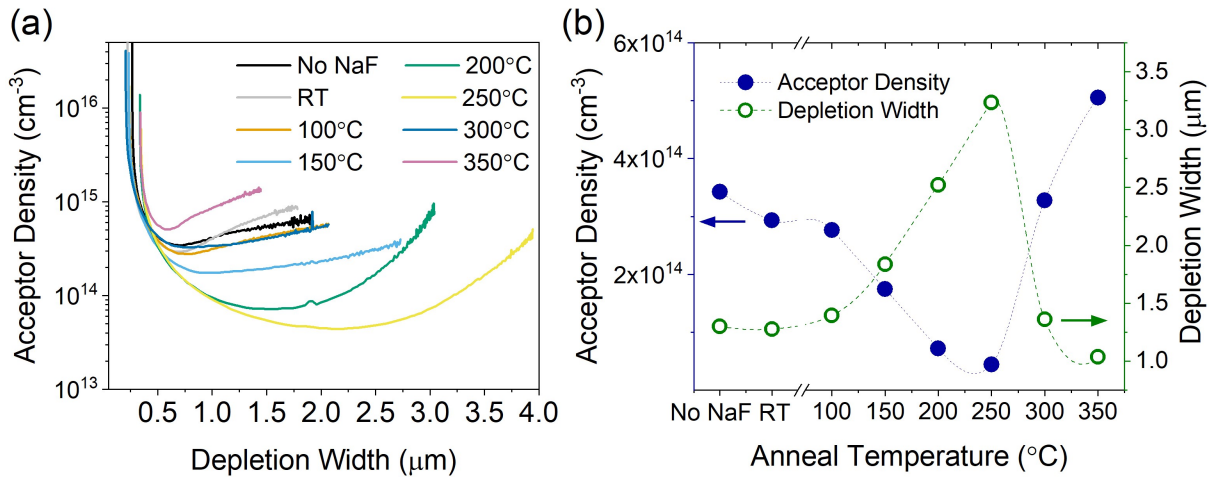


Figure 4: (a) Acceptor density versus depletion width extracted from Mott-Schottky plots for devices with 1 nm NaF annealed up to 350°C compared to a device without NaF, (b) bulk acceptor density taken from the minima of curves in Figure 4a, and the depletion width at zero bias

174 volume of CdTe to balance the overall charge. The change in depletion width with anneal temperature can be seen
 175 to roughly match the trend in Figure 3d which can explain the improvement in EQE response at long wavelengths
 176 up to 250°C. Devices which have the largest depletion width allow more efficient collection of carriers further
 177 into the device, which long wavelength photons are more likely to reach. Since depletion width scales inversely
 178 with acceptor concentration, it is necessary to find a balance between a highly doped absorber to increase V_{oc} ,
 179 whilst maintaining a sufficient electric field in the bulk of the device. That balance depends on a range of material
 180 properties such as carrier lifetime, mobility and absorber thickness, and is typically around 10^{16} cm^{-3} for CdTe
 181 [26]. This is much higher than observed here and therefore despite the reduced depletion width, annealing devices
 182 with NaF above 250°C is likely necessary for effective doping.

183 3.2. Chemical composition of NaF treated devices

184 Having looked at how annealing NaF affects CdTe at a device level, the effect of processing conditions on the
 185 elemental profiles and back surface is now considered. The anneal temperature has been found to influence the
 186 extent of sodium incorporation into the device, with temperatures above 250°C required to increase the carrier
 187 concentration. A control device without NaF or annealing was compared to devices with 1 nm NaF annealed
 188 for 20 min in air at either low (200°C) or high (300°C) temperature. Figure 5 shows the distribution of sodium,
 189 fluorine and chlorine measured via ToF-SIMS analysis and quantified by comparing these devices to ion-implanted
 190 reference standards for each element in CdTe.

191 Sodium is present in significant quantities in the control device without the intentional addition of NaF. There
 192 are several potential sources of sodium, as described further in Section 3.3, and the concentration of $\sim 10^{17} \text{ cm}^{-3}$
 193 in the bulk of the CdTe layer is consistent with previously reported values [27–29]. Upon the addition of 1 nm NaF
 194 at the back surface and annealing at 200 °C there is a large increase in the sodium signal at the back surface, which
 195 gradually decreases further into the bulk following a typical in-diffusion profile, before increasing again at the
 196 front on the device near the CdS layer. The Te rich back surface resulting from the NP etch [30] may account for
 197 the relative ease of incorporation at the back contact, however sodium does not appear to incorporate effectively

198 into the bulk of the CdTe with only a minor increase in comparison to the control device. Nonetheless it would
199 appear to be mobile throughout the device, since there is increased accumulation at the front surface towards the
200 CdS window layer. This could be accounted for if transport is dominated by rapid diffusion along grain boundaries
201 which is expected to be far quicker than through the grain interior [31]. This would allow sodium to reach the
202 CdS layer relatively easily, where its effect on device performance remains unclear. Sodium would be expected
203 to compensate native *n*-type CdS doping by occupying a cadmium site through the formation of Na_{Cd} acceptors,
204 which would lower the built-in voltage (V_{bi}) due to a lower net doping density. However, CdS is natively *n*-type
205 due to sulphur vacancies [32] and therefore it is unclear whether this Cd rich composition would lend itself to the
206 formation of Na_{Cd} acceptors or would sit interstitially. Nonetheless it appears that, similar to copper [3], sodium
207 shows a strong preference to segregate at the junction position, consistent with previous observations by other
208 authors [29].

209 For the 300°C annealed sample there is a further increase in sodium content at the front contact, however there
210 is also a near-uniform incorporation throughout the bulk CdTe. This indicates that the higher anneal temperature
211 is required to drive the sodium into the grain interior, which would be consistent with the sharp change in the trend
212 of doping density observed at this temperature in Figure 4. There is also a small peak in the sodium profile near
213 the back surface for the 300°C anneal, which again could result from Na incorporating more effectively in the Te
214 rich region left by the NP etch, or alternatively be due to a difference in sputtering yield due to surface oxidation.

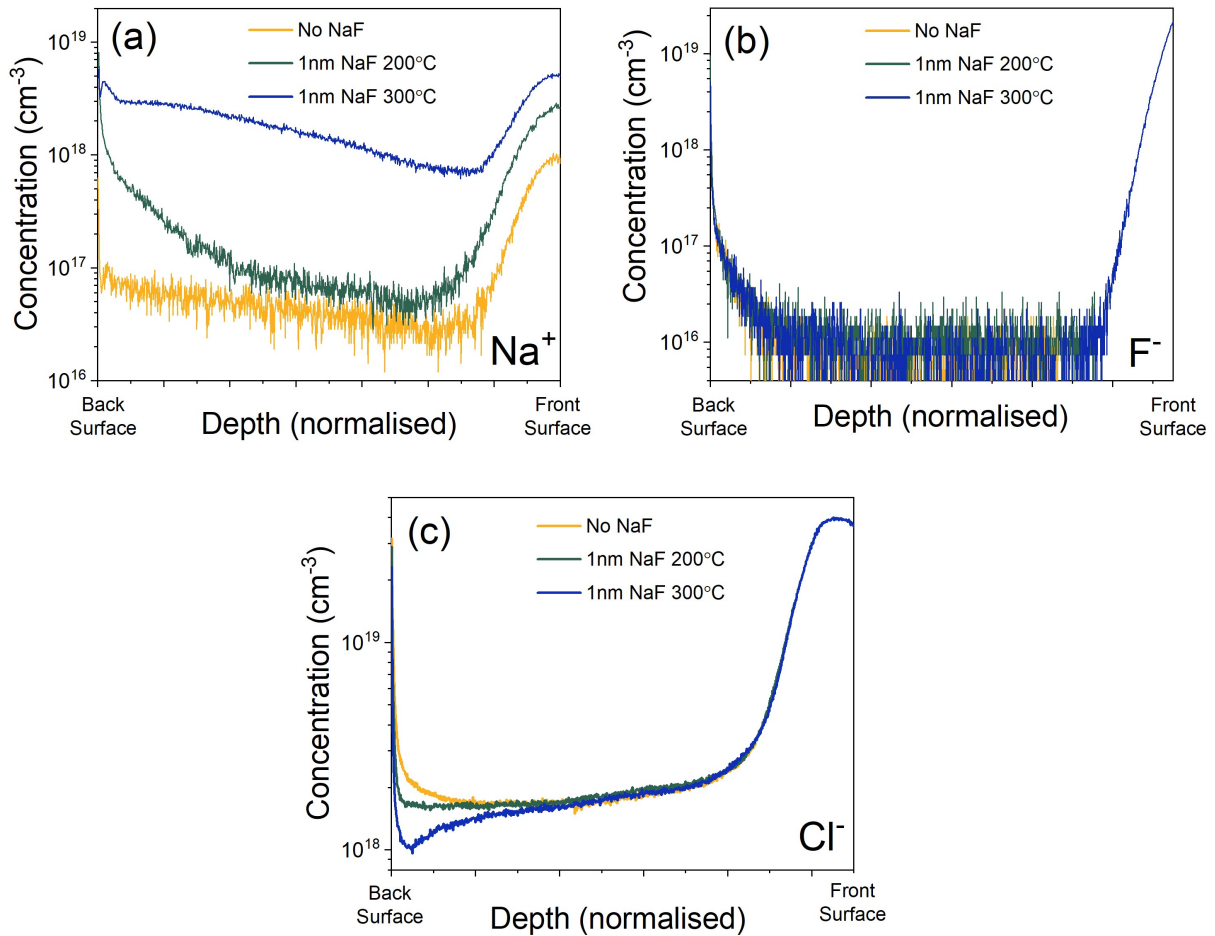


Figure 5: Distribution of (a) sodium, (b) fluorine and (c) chlorine obtained from ToF-SIMS measurements of devices with 1 nm NaF deposited following MgCl₂ treatment annealed at 200°C and 300°C compared to a reference device without NaF.

215 The fluorine signal shown in Figure 5b shows an identical trend for all three devices regardless of the addition
 216 of NaF or the anneal temperature. Whilst fluorine would be expected to be an *n*-type dopant in CdTe when
 217 occupying Te sites, chlorine is in the same group and appears to aid *p*-type doping via the formation of the
 218 shallow A-centre defect complex $(V_{Cd} - Cl_{Te})^{-1}$ [33][34]. It is unclear whether fluorine would act in a similar
 219 manner, although it is noteworthy that there is preliminary evidence of fluorine inclusion during chlorine treatment
 220 having a beneficial effect [35, 36]. In any case, the absence of any additional fluorine from the NaF treatment is
 221 favourable for achieving a high doping density with a simpler defect structure, and suggests NaF is a suitable
 222 source of sodium. Diffusion of fluorine into CIGSSe solar cells during NaF treatment is inhibited by the formation
 223 of volatile SeF₆ [37]. A similar reaction to form TeF₆ might occur here and would offer a plausible explanation
 224 for the lack of excess F signal in the bulk of the CdTe layer upon NaF treatment. Despite no additional fluorine
 225 contribution in the CdTe layer from the NaF layer within the instrumental detection limits, there is a clear increase
 226 in signal towards the back surface for all devices. This could result from out-diffusion from the SnO₂:F layer at the
 227 front contact, whereby fluorine segregates out of the CdTe layer towards the back surface during device processing
 228 as seen previously by Emziane et al [38]. Impurities in the MgCl₂ solution and NP etch could also offer potential
 229 sources of fluorine contamination.

230 Figure 5c shows a similar chlorine content for the three devices towards the front surface and most of the bulk
231 CdTe layer, however there is a small change at the back surface for the three devices. All samples show a very rapid
232 increase in chlorine concentration within the first few nanometres from the back contact which likely indicates
233 oxychlorides remaining on the surface following the activation treatment [39]. The control device without NaF
234 shows a large, gradual increase in Cl concentration at the back surface which is not surprising given the MgCl_2
235 activation process is likely to leave a chlorine rich region. The low temperature NaF annealed device shows a
236 much flatter region with no gradual increase in Cl signal. Higher anneal temperature leads to a further reduction
237 of the back-surface Cl content, leaving a slightly chlorine deficient region. It is unclear what causes this loss
238 of chlorine and whether it has an impact on device performance, but since the chlorine deficient regions overlap
239 with the excess sodium, some reaction involving both elements seems plausible. Considering the improvement
240 in contacting with NaF implied in Figure 1, this change in chemical composition at the back surface could be
241 beneficial for device performance.

242 XPS was used to determine the chemical composition of the back surface of a reference CdTe device without
243 NaF compared to one with 1 nm NaF deposited prior to a 20 min anneal at 300°C in air, which was expected to
244 show the most significant change from previous analysis. The $3d_{5/2}$ core level peaks are given in Figure 6 (a) for Cd
245 and (b) for Te. The cadmium spectra in both cases can be fit with a single peak and therefore atoms are bonded only
246 to tellurium with no contribution from sodium, fluorine, magnesium, or chlorine (within the limits of detection).
247 While the tellurium peak for the reference device is similar, in that there is only one bonding environment, in
248 the case of the NaF device there is a secondary peak appearing at higher binding energy corresponding to the
249 formation of a TeO_2 oxide phase at the back surface. This oxidation is caused by the annealing step required
250 to effectively distribute the sodium throughout the CdTe and increase the doping density, however is likely to be
251 detrimental to device performance as it will hinder the formation of an ohmic contact [40, 41]. In this case it
252 appears the beneficial effects of doping outweigh the effects of this oxidation as this does not show the rollover
253 observed for the reference device in Figure 1, however the series resistance does increase with anneal temperature
254 which is likely caused by increasing the thickness of TeO_2 . This might be overcome by annealing the devices
255 either in an inert atmosphere or under vacuum, so that high doping densities might be obtained as well as an oxide
256 free surface.

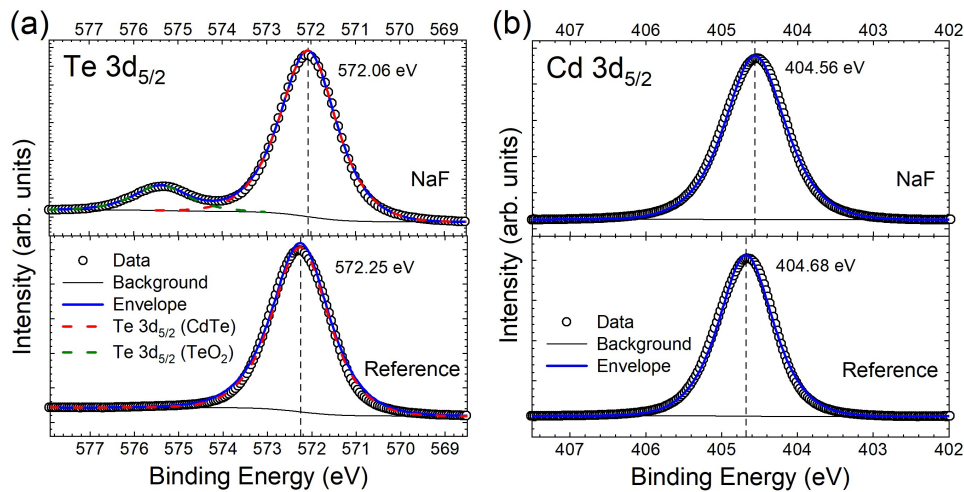


Figure 6: Core level XPS spectra showing the (a) Te $3d_{5/2}$ and (b) Cd $3d_{5/2}$ peaks comparing a standard CdTe device to one with 1 nm NaF evaporated at the back surface and annealed at 300°C for 20 min in air

257 3.3. Unintentional sodium in CdTe solar cells

258 The presence of unintentional dopants in source materials can have a significant influence photovoltaic device
 259 performance, and have been documented to go as far as changing the carrier type of absorber materials from p -
 260 type to n -type [42]. Whilst copper is typically considered to be a common impurity even in nominally undoped
 261 CdTe films [4], since tellurium is manufactured as a byproduct of copper refinement, far less attention is paid to
 262 the sodium contamination. However, given the measurement of $> 10^{16} \text{ cm}^{-3}$ Na atoms in 'NaF free' reference
 263 devices (Figure 5a), it is important to consider the potential sources of unintentional sodium incorporation during
 264 device processing. Impurity analysis via ICP-OES of the 5N purity (Alfa Aesar) CdTe source material used in this
 265 work is detailed in Table S1, and shows sodium to be present in a concentration of $(4.2 \pm 0.2) \times 10^{17} \text{ cm}^{-3}$. This is
 266 much higher than for copper, which was barely detected on the limits of the instrument implying a concentration
 267 around $\sim 10^{14} \text{ cm}^{-3}$. Sodium has previously been shown to strongly affect the electronic and structural properties
 268 of CdTe films [14, 16], yet there are few reports considering what role this level of contamination might play in a
 269 device structure.

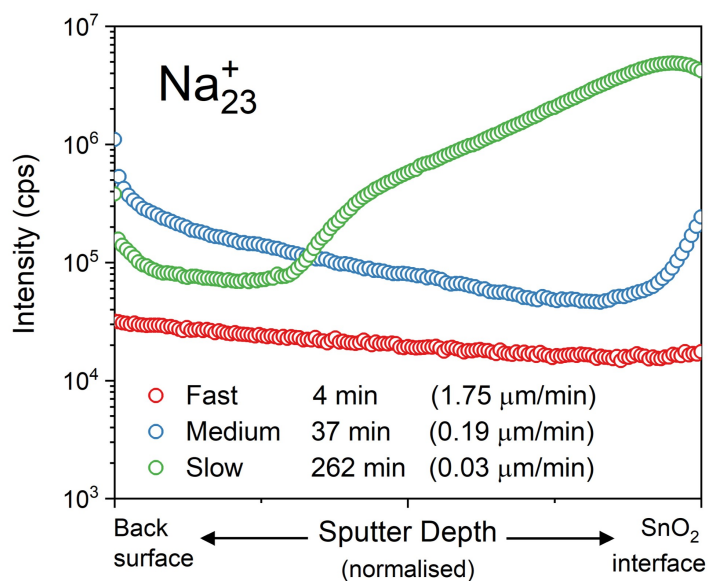


Figure 7: SIMS depth profile showing the relative distribution of sodium in CdTe films grown on TEC15M substrates at different growth rates, thereby exposing the substrates to high temperatures (550°C) for 4 min (fast), 37 min (medium) and 262 min (slow) during deposition

270 Although impurities within the source material might be avoided relatively easily with further purification of
 271 CdTe, other sources of contamination such as diffusion from glass substrates may be more challenging to prevent
 272 whilst remaining compatible with low-cost, high-volume manufacturing. Figure S6 shows a CdTe film deposited
 273 onto a TEC 15M substrate, which consists of soda lime glass coated with series of layers, including a nominally
 274 30nm SiO₂ film which acts as an alkali diffusion barrier layer [43]. Such substrates are ubiquitous in CdTe
 275 literature as they are convenient, low-cost and produced commercially in high volumes. The ability of the SiO₂
 276 layer to effectively prevent out-diffusion of sodium was examined by depositing CdTe onto these substrates at
 277 different growth rates, thereby varying the amount of time the samples are subject to elevated temperatures. This
 278 was achieved by adjusting the chamber pressure during CSS deposition, which in turn changes the sublimation
 279 rate and therefore controls the CdTe growth rate [20]. During this time, the substrate is held at 550°C, which is
 280 typical for CdTe processing to encourage a large grain structure.

281 Figure 7 shows the distribution of sodium throughout a CdTe film deposited on TEC 15M substrates at three
 282 different growth rates, measured via non-quantitative SIMS profiling. Fast deposition (4 mins) of the CdTe layer
 283 results in uniform incorporation of sodium throughout the absorber layer, with a slight decrease in signal intensity
 284 as the measurement proceeds from the back surface of the CdTe layer towards the SnO₂ substrate. As the growth in
 285 slowed down to a 37 min deposition, the count rate of the sodium ions increases by roughly an order of magnitude,
 286 with a sharp increase towards the SnO₂ layer suggesting out-diffusion from the substrate. This is in agreement
 287 with observations by Emziane *et al* who found comparable levels of sodium contamination in CdTe films, which
 288 was similarly ascribed to diffusion from the glass substrates [29, 38]. Further slowing the growth rate leads to a
 289 large increase in the sodium content in the bulk CdTe region close to the substrate, decreasing towards the back
 290 surface. The increased count rate for longer depositions, especially towards the substrate interface, shows that
 291 slowing the growth rate the increases the concentration of sodium in the CdTe layer. This is presumably due to
 292 more impurity diffusion out of the soda-lime glass caused by the higher thermal budget of the deposition process.

293 Although CSS grown CdTe layers are typically deposited at high growth rates, this demonstrates the potential
294 for sodium migration from glass substrates despite the use of alkali blocking layers. Whilst sodium is expected
295 to increase *p*-type doping and therefore may be beneficial to device performance, uncontrolled incorporation
296 from source material and diffusion during processing is not likely to be an effective, nor reproducible, doping
297 strategy. Instead we have found that depositing a thin layer of NaF at the back surface of CdTe solar cells prior to
298 metallisation, analogous to how copper is often incorporated, offers a controllable method of sodium incorporation.
299 However, given the already considerable levels of sodium present in the control devices, additional study of CdTe
300 devices deposited on alkali free substrates with higher purity source material would allow the effect of sodium to
301 be isolated further.

302 **4. Conclusions**

303 Sodium has been shown to be present in significant quantities for CdTe samples of commercially available
304 5N polycrystalline lumps, as well as in thin films deposited onto soda lime glass due to out-diffusion from the
305 substrate. Given sodium is an active *p*-type dopant in CdTe, this work highlights the importance of identifying
306 unintentional impurities and the role they may have in CdTe solar cells.

307 The evaporation of a thin layer of NaF prior to contacting CdTe solar cells has been shown to be an effective
308 strategy for intentionally incorporating sodium into the device structure without the adverse structural effects
309 observed by previous authors [14, 16–18]. However, the improvement in device performance has been modest
310 even for optimised treatment conditions. This is likely due to several overlapping processes occurring during
311 the evaporation of NaF and subsequent annealing of devices, such as oxidation of the back contact and sodium
312 accumulation in the CdS layer. It may also be that given the high sodium content already present in the control
313 device, the additional sodium is of limited benefit to device efficiency overall. However, at the back surface an
314 improved contact is readily achievable regardless of specific processing steps, requiring only the presence of 1 nm
315 NaF. This produces a highly doped region at the back surface which thereby lowers the contact barrier, leading to
316 an increased fill factor due to lower series resistance. Increasing the bulk doping density requires annealing devices
317 to redistribute the sodium throughout the device, and from the grain boundaries into the grain interior. This occurs
318 for annealing temperatures above 300°C, whereby the doping density increases above that of the reference device.
319 Optimised processing conditions lead to a minor overall improvement for devices annealed at 300°C compared to
320 a reference device without NaF, which is primarily a result of an increased fill factor caused by an improved back
321 contact. This work highlights the importance of sodium as impurity in CdTe solar cells, and shows the potential
322 for intentional sodium doping to improve device performance without recrystallisation of the CdTe layer.

323 **5. Supplementary Information**

324 JV performance parameters and CV measurements of CdTe devices with different NaF thickness, JV data for
325 stability of devices over two month period, XRD of NaF coated CdTe films as a function of anneal temperature,
326 electron microscopy of CdTe films with and without NaF, ICP-OES of CdTe source material, cross section electron
327 microscopy of CdTe/TEC15M device stack.

328 6. Corresponding Author

329 jon.major@liverpool.ac.uk

330 7. Author Contributions

331 TPS fabricated samples and prepared the manuscript with JDM. HS and VRD conducted XPS analysis. OSH
332 and GZ carried out SIMS measurements while electron microscopy was performed by LB.

333 8. Acknowledgements

334 The authors gratefully acknowledge Prof Tim Veal for help with interpretation of XPS data, Dr Stephen Camp-
335 bell for supporting measurements on related samples and Dr Sarah Fearn for assistance with ToF SIMS measure-
336 ments. Additionally, the SEM SRF Albert Crewe Centre for Electron Microscopy is thanked for access to their
337 facilities.

338 9. Funding Sources

339 Funding for the work was provided by EPSRC via EP/R021503, EP/N014057/1 and EP/L01551X/1.

340 References

- 341 [1] M. A. Green, E. D. Dunlop, J. Hohl-Ebinger, M. Yoshita, N. Kopidakis, X. Hao, Solar cell efficiency tables (version 58), *Progress in*
342 *Photovoltaics: Research and Applications* 29 (2021) 657–667.
- 343 [2] E. Artegiani, D. Menossi, H. Shiel, V. Dhanak, J. D. Major, A. Gasparotto, K. Sun, A. Romeo, Analysis of a novel CuCl₂ back contact
344 process for improved stability in CdTe solar cells, *Progress in Photovoltaics: Research and Applications* 27 (2019) 706–715.
- 345 [3] C. Corwine, A. Pudov, M. Gloeckler, S. Demtsu, J. Sites, Copper inclusion and migration from the back contact in CdTe solar cells,
346 *Solar Energy Materials and Solar Cells* 82 (2004) 481–489.
- 347 [4] C. Jenkins, A. Pudov, M. Gloeckler, S. Demtsu, T. Nagle, A. Fahrenbruch, CdTe back contact: Response to copper addition and
348 out-diffusion, *NCPV and Solar Program Review Meeting* (2003).
- 349 [5] A. Nagaoka, K. Nishioka, K. Yoshino, R. Katsube, Y. Nose, T. Masuda, M. A. Scarpulla, Comparison of Sb, As, and P doping in Cd-
350 rich CdTe single crystals: Doping properties, persistent photoconductivity, and long-term stability, *Applied Physics Letters* 116 (2020)
351 132102.
- 352 [6] T. Ablekim, S. Swain, W.-J. Yin, K. Zaunbrecher, J. Burst, T. Barnes, D. Kuciauskas, S.-H. Wei, K. Lynn, Self-compensation in arsenic
353 doping of CdTe, *Scientific Reports* 7 (2017) 4533.
- 354 [7] W. Metzger, S. Grover, D. Lu, E. Colegrove, J. Moseley, C. Perkins, X. Li, R. Mallick, W. Zhang, R. Malik, J. Kephart, C.-S. Jiang,
355 D. Kuciauskas, D. Albin, M. Al-Jassim, G. Xiong, M. Gloeckler, Exceeding 20% efficiency with in situ group V doping in polycrystalline
356 CdTe solar cells, *Nature Energy* 4 (2019) 1–9.
- 357 [8] D. Li, C. Yao, V. Sankaranarayanan Nair, R. Awni, K. Khanal Subedi, R. Ellingson, L. Li, Y. Yan, F. Yan, Low-temperature and effective
358 ex situ group V doping for efficient polycrystalline CdSeTe solar cells, *Nature Energy* 6 (2021) 1–8.
- 359 [9] R. J. Hand, D. R. Tadjiev, Mechanical properties of silicate glasses as a function of composition, *Journal of Non-Crystalline Solids* 356
360 (2010) 2417–2423. 12th International Conference on the Physics of Non-Crystalline Solids (PNCS 12).
- 361 [10] Y. Yan, X. Li, R. Dhere, M. Al-Jassim, K. Jones, M. Young, M. Scott, SiO₂ as barrier layer for Na out-diffusion from soda-lime glass,
362 in: 2010 35th IEEE Photovoltaic Specialists Conference, pp. 002519–002521.
- 363 [11] J. D. Major, L. Bowen, K. Durose, Focussed ion beam and field emission gun–scanning electron microscopy for the investigation of
364 voiding and interface phenomena in thin-film solar cells, *Progress in Photovoltaics: Research and Applications* 20 (2012) 892–898.

- 365 [12] S.-H. Wei, S. B. Zhang, Chemical trends of defect formation and doping limit in II-VI semiconductors: The case of CdTe, *Phys. Rev. B*
366 66 (2002) 155211.
- 367 [13] J. N. Duenow, J. M. Burst, D. S. Albin, D. Kuciauskas, S. W. Johnston, R. C. Reedy, W. K. Metzger, Single-crystal CdTe solar cells with
368 V_{oc} greater than 900mV, *Applied Physics Letters* 105 (2014) 053903.
- 369 [14] L. Kranz, J. Perrenoud, F. Pianezzi, C. Gretener, P. Rossbach, S. Buecheler, A. Tiwari, Effect of sodium on recrystallization and
370 photovoltaic properties of CdTe solar cells, *Solar Energy Materials and Solar Cells* 105 (2012) 213–219.
- 371 [15] K. Durose, D. Albin, R. Ribelin, R. Dhere, D. King, H. Moutinho, R. Matson, P. Dippo, J. Hiie, D. Levi, The influence of NaCl on the
372 microstructure of CdS films and CdTe solar cells, in: *Microscopy of Semiconducting Materials 1999, Proceedings*, 164, pp. 207–210.
- 373 [16] A. Amirghalili, V. Barrioz, S. J. Irvine, N. S. Beattie, G. Zoppi, A combined Na and Cl treatment to promote grain growth in MOCVD
374 grown CdTe thin films, *Journal of Alloys and Compounds* 699 (2017) 969–975.
- 375 [17] R. Dhere, K. Ramanathan, J. Keane, J. Zhou, H. Moutinho, S. Asher, R. Noufi, Effect of Na incorporation on the growth and properties
376 of CdTe/CdS devices, in: *Conference Record of the Thirty-first IEEE Photovoltaic Specialists Conference, 2005.*, pp. 279–282.
- 377 [18] T. P. Shalvey, J. D. Major, Impact of NaF during chloride treatment of CdTe solar cells, *Materials Science in Semiconductor Processing*
378 107 (2020) 104827.
- 379 [19] J. D. Major, R. E. Treharne, L. J. Phillips, K. Durose, A low-cost non-toxic post-growth activation step for CdTe solar cells, *Nature* 511
380 (2014) 334+.
- 381 [20] J. Major, Y. Proskuryakov, K. Durose, G. Zoppi, I. Forbes, Control of grain size in sublimation-grown CdTe, and the improvement in
382 performance of devices with systematically increased grain size, *Solar Energy Materials and Solar Cells* 94 (2010) 1107–1112.
- 383 [21] J. Major, L. Phillips, M. Al Turkestani, L. Bowen, T. Whittles, V. Dhanak, K. Durose, P3HT as a pinhole blocking back contact for CdTe
384 thin film solar cells, *Solar Energy Materials and Solar Cells* 172 (2017) 1–10.
- 385 [22] E. Artegiani, D. Menossi, H. Shiel, V. Dhanak, J. D. Major, A. Gasparotto, K. Sun, A. Romeo, Analysis of a novel CuCl_2 back contact
386 process for improved stability in CdTe solar cells, *Progress in Photovoltaics: Research and Applications* 27 (2019) 706–715.
- 387 [23] A. Niemegeers, M. Burgelman, Effects of the Au/CdTe back contact on IV and CV characteristics of Au/CdTe/CdS/TCO solar cells,
388 *Journal of Applied Physics* 81 (1997) 2881–2886.
- 389 [24] S. Hegedus, B. McCandless, R. Birkmire, Analysis of stress-induced degradation in CdS/CdTe solar cells, in: *Conference Record of the*
390 *Twenty-Eighth IEEE Photovoltaic Specialists Conference - 2000*, pp. 535–538.
- 391 [25] B. L. Crowder, W. N. Hammer, Shallow acceptor states in ZnTe and CdTe, *Phys. Rev.* 150 (1966) 541–545.
- 392 [26] A. Kanevce, T. A. Gessert, Optimizing CdTe solar cell performance: Impact of variations in minority-carrier lifetime and carrier density
393 profile, *IEEE Journal of Photovoltaics* 1 (2011) 99–103.
- 394 [27] K. Durose, M. Cousins, D. Boyle, J. Beier, D. Bonnet, Grain boundaries and impurities in CdTe/CdS solar cells, *Thin Solid Films*
395 403-404 (2002) 396–404. *Proceedings of Symposium P on Thin Film Materials for Photovoltaics*.
- 396 [28] D. Halliday, M. Emziane, K. Durose, A. Bosio, N. Romeo, Effects of impurities in CdTe/CdS structures: Towards enhanced device
397 efficiencies, in: *2006 IEEE 4th World Conference on Photovoltaic Energy Conference*, volume 1, pp. 408–411.
- 398 [29] M. Emziane, K. Durose, N. Romeo, A. Bosio, D. P. Halliday, A combined SIMS and ICPMS investigation of the origin and distribution of
399 potentially electrically active impurities in CdTe/CdS solar cell structures, *Semiconductor Science and Technology* 20 (2005) 434–442.
- 400 [30] X. Li, D. W. Niles, F. S. Hasoon, R. J. Matson, P. Sheldon, Effect of nitric-phosphoric acid etches on material properties and back-contact
401 formation of CdTe-based solar cells, *Journal of Vacuum Science & Technology A* 17 (1999) 805–809.
- 402 [31] J. D. Poplawsky, C. Li, N. R. Paudel, W. Guo, Y. Yan, S. J. Pennycook, Nanoscale doping profiles within CdTe grain boundaries and
403 at the CdS/CdTe interface revealed by atom probe tomography and STEM EBIC, *Solar Energy Materials and Solar Cells* 150 (2016)
404 95–101.
- 405 [32] N. Maticiuc, N. Spalatu, V. Mikli, J. Hiie, Impact of cds annealing atmosphere on the performance of cds–cdte solar cell, *Applied*
406 *Surface Science* 350 (2015) 14–18. *SATF2014 : Science and Applications of Thin Films, Conference & Exhibition*.
- 407 [33] D. M. Hofmann, P. Omling, H. G. Grimmeiss, B. K. Meyer, K. W. Benz, D. Sinerius, Identification of the chlorine A center in CdTe,
408 *Phys. Rev. B* 45 (1992) 6247–6250.
- 409 [34] N. Spalatu, M. Krunk, J. Hiie, Structural and optoelectronic properties of cdcl2 activated cdte thin films modified by multiple thermal
410 annealing, *Thin Solid Films* 633 (2017) 106–111. *E-MRS 2016 Spring Meeting, Symposium V, Thin-Film Chalcogenide Photovoltaic*
411 *Materials*.
- 412 [35] N. Romeo, A. Bosio, V. Canevari, A. Podestà, Recent progress on CdTe/CdS thin film solar cells, *Solar Energy* 77 (2004) 795–801.

- 413 [36] S. Mazzamuto, L. Vaillant, A. Bosio, N. Romeo, N. Armani, G. Salviati, A study of the CdTe treatment with a Freon gas such as CHF₂Cl,
414 Thin Solid Films 516 (2008) 7079–7083.
- 415 [37] A. Laemmle, R. Wuerz, T. Schwarz, O. Cojocaru-Mirédin, P.-P. Choi, M. Powalla, Investigation of the diffusion behavior of sodium in
416 Cu(In,Ga)Se₂ layers, Journal of Applied Physics 115 (2014) 154501.
- 417 [38] M. Emziane, K. Durose, D. Halliday, N. Romeo, A. Bosio, SIMS depth profiling of CdTe-based solar cells grown on sapphire substrates,
418 Thin Solid Films 511-512 (2006) 66–70.
- 419 [39] D. Waters, D. Niles, T. Gessert, D. Albin, D. Rose, P. Sheldon, C. Blvd, Surface analysis of CdTe after various pre-contact treatments,
420 in: 2nd World Conference and Exhibition on Photovoltaic Solar Energy Conversion, Vienna, pp. 530–23876.
- 421 [40] V. P. Singh, O. M. Erickson, J. H. Chao, Analysis of contact degradation at the CdTe-electrode interface in thin film CdTe-CdS solar
422 cells, Journal of Applied Physics 78 (1995) 4538–4542.
- 423 [41] M. O. Reese, J. M. Burst, C. L. Perkins, A. Kanevce, S. W. Johnston, D. Kuciauskas, T. M. Barnes, W. K. Metzger, Surface passivation
424 of CdTe single crystals, IEEE Journal of Photovoltaics 5 (2015) 382–385.
- 425 [42] T. D. C. Hobson, L. J. Phillips, O. S. Hutter, H. Shiel, J. E. N. Swallow, C. N. Savory, P. K. Nayak, S. Mariotti, B. Das, L. Bowen,
426 L. A. H. Jones, T. J. Featherstone, M. J. Smiles, M. A. Farnworth, G. Zoppi, P. K. Thakur, T.-L. Lee, H. J. Snaith, C. Leighton, D. O.
427 Scanlon, V. R. Dhanak, K. Durose, T. D. Veal, J. D. Major, Isotype heterojunction solar cells using n-type Sb₂Se₃ thin films, Chemistry
428 of Materials 32 (2020) 2621–2630.
- 429 [43] P. Koirala, J. Li, H. P. Yoon, P. Aryal, S. Marsillac, A. A. Rockett, N. J. Podraza, R. W. Collins, Through-the-glass spectroscopic ellip-
430 sometry for analysis of CdTe thin-film solar cells in the superstrate configuration, Progress in Photovoltaics: Research and Applications
431 24 (2016) 1055–1067.